Nanoscale Horizons

ROYAL SOCIETY OF CHEMISTRY

COMMUNICATION

View Article Online
View Journal | View Issue

Open Access Article. Published on 14 August 2025. Downloaded on 1/24/2026 11:41:00 PM.
This article is licensed under a Creative Commons Attribution 3.0 Unported Licence.

Check for updates

Cite this: *Nanoscale Horiz.*, 2025, **10**, 2607

Received 22nd April 2025,
Accepted 6th August 2025

DOI: 10.1039/d5nh00263j

rsc.li/nanoscale-horizons

# FluMag-SELEX derived specific individual aptamers can fluorescently label the ageing immanent protein-crosslinker glucosepane in diabetic mouse tissues

Runliu Li,[a] Bastian Draphoen,[b] Mika Lindén,[b] Karmveer Singh,[c] Karin Scharffetter-Kochanek,[c] Andreas Stürmer,[d] Frank Rosenau*[a] and Ann-Kathrin Kissmann*[ae]

**Nowadays, aptamers have transitioned into valuable antibody alternatives. We present the first anti-glucosepane aptamer targeting a key glycation product linked to aging and diabetes. Glu3, with high specificity and affinity, enabled the first-ever direct, fluorescence-based histological staining of glucosepane in murine tissue, distinguishing diabetic samples from wild-type samples without secondary reagents.**

## Introduction

Beginning with the pioneering research by the Szostak and Gold groups in 1990,[1,2] which introduced nucleic acid-based affinity molecules, more than three decades of extensive fundamental research on these "aptamers" have relieved current scientists from needing to test and establish all over again the basic suitability of these molecules. Instead, the concept of aptamers has advanced to the point where it is now a viable technology for real-world applications in diagnostics and pharmaceutical biotechnology. The core methodology behind a typical aptamer project involves the evolution and selection of effective DNA or RNA oligonucleotides ("aptamers") with the desired affinity and specificity for a given target. Today, numerous variations of the SELEX process ("Systematic Evolution of Ligands by EXponential enrichment") exist, each tailored for different types of targets, ranging from small molecules (such as "Capture-SELEX")[3–5] to proteins, whole cells, and tissues from humans, animals, or plants.[6–12] The introduction of FluMag-SELEX[13] represented a significant advancement, making the process more experimentally manageable and allowing for step-by-step monitoring and measurements. This version of SELEX uses fluorescently labeled aptamers throughout the process, enabling the labeling of the target immobilized on magnetic particles by freshly isolated sub-libraries after each round.[13] As a result, direct quantitative measurements can be taken using fluorimeters or a fluorescence microscope. FluMag-SELEX is generally considered most suitable for larger molecules, such as proteins[13–16] or other molecules[17] that can easily be immobilized on magnetic particles.

### New concepts

Aptamers have evolved from a principally questionable concept three decades ago to an accepted class of binding molecules nowadays replacing antibodies in a variety of technologies. Every additional new application adds an additional piece of reliability of aptamer-based detection technologies and improves their spectrum of possible applications. The next relevant analyte, glucosepane, is a lysine–arginine protein crosslink and an advanced glycation end product derived from D-glucose. Glucosepane is closely related to aging, plays a central role in diabetes and has been associated with severe tissue dysfunction. Here, we developed a focused aptamer-library in a FluMag-SELEX process over 6 selection rounds, identified 10 individual aptamers and characterized their performance. Besides being functional in fluorescent labelling of glucosepane on magnetic particles and its purification from solutions, the "best-performer" aptamer Glu3 showed a low nanomolar dissociation constant allowing staining of mouse skin tissue sections. This aptamer-mediated histological staining allowed specific discrimination of samples from diabetic mice and wild-type mice in direct fluorescent labelling without the need for additional secondary antibodies or (enzyme-)conjugates. Moreover, this new staining procedure was fast and easy with a total duration of ~2.5 hours. We have introduced the first anti-glucosepane aptamer and have also added another example to the portfolio of histological staining procedures. The ease of aptamer selection in the SELEX process as well as the ease of the aptamer-based histological staining procedure without secondary binding molecules not only make this complete developmental work-flow unprecedentedly fast, but also promise high economic affordability of future aptamer-based staining-technologies.

[a] Institute of Pharmaceutical Biotechnology, Ulm University, Albert-Einstein-Allee 11, 89081 Ulm, Germany. E-mail: ann-kathrin.kissmann@uni-ulm.de
[b] Institute of Inorganic Chemistry II, Ulm University, Albert-Einstein-Allee 11, 89081 Ulm, Germany
[c] Department of Dermatology and Allergic Diseases, Ulm University, Albert-Einstein-Allee 11, 89081 Ulm, Germany
[d] T-Technologies Grundlagenforschung e.U., Sonntagberg 10, 4550 Kremsmünster, Austria
[e] Danube Private University, Steiner Landstraße 124, Krems an der Donau 3500, Austria

Open Access Article. Published on 14 August 2025. Downloaded on 1/24/2026 11:41:00 PM.
This article is licensed under a Creative Commons Attribution 3.0 Unported Licence.

In addition to their use as recognition elements in sensing applications as on electronic biosensors,[14,18,19] aptamers can be used in traditional diagnostics techniques and in rare cases have shown their potential in immunohistological staining, *e.g.* by labeling *Candida albicans* cells in paraffin-embedded sections of rat tissues.[20] Nevertheless, binding molecules have been used by far most frequently for decades and still antibodies are directed against the respective target in combination with secondary antibodies providing fluorescent labels or enzymes for colori-/fluorogenic signal enhancement techniques.[21,22]

Glucosepane is formed by a non-enzymatic reaction between free glucose in tissues and the side chains of lysine and arginine and glucosepane is referred to as an "advanced glycation end product" (AGE) derived from D-glucose and probably represents the most important AGE in general.[23,24] Glucosepane is the core structural component of protein-crosslinking products and may serve as an example for "non-productive" (*i.e.* prone with negative health consequences) glycosylation in the human body. It is an irreversible covalent cross-linked product that has been found to form intermolecular and intramolecular cross-links in the extracellular matrix (ECM) of collagen and crystalline proteins of the eye.[25–28] Although structurally it is a small molecule, its importance lies in its function as a stable AGE cross-link within long-lived proteins. Glucosepane has been the richest protein cross-link found in the body to date, with its content in human tissues being 10 to 1000 times of that of any other cross-linked AGE and hence is currently considered the most important AGE.[29–31] Glucosepane is present in human tissues at levels 10 to 1000 times higher than any other cross-linking AGE, and is currently considered to be the most important cross-linking AGE. As the content of glucosepane increases with age[32–34] and by increasing the stiffness of collagen, glucosepane cross-linking may have significant implications for several age-related diseases, such as cardiovascular disease, diabetes, and osteoporosis.[35–37] While the formation pathways of glucosepane are relatively well understood, the accumulation and pathophysiology of glucosepane remain unclear. AGE formation in diabetes is increasingly important as a marker and potential culprit of diabetes complications, particularly retinopathy, kidney disease, and neuropathy. Over the years, relevant studies have successfully revealed that glucosepane is a causative factor of diabetic retinopathy, nephropathy, and neuropathy, and a cofactor of cardiovascular diseases in various animal models.[38] Monnier's group's research on glucosepane showed that the level of glucosepane crosslinking in the human collagen in the ECM increases gradually with age, and more rapidly in people with diabetes, thus indicating the role of glucosides in the long-term effects associated with diabetes and aging, such as atherosclerosis, joint stiffness, and skin wrinkling.[39,40] Aging is undoubtedly one of the most important and yet unsolved problems of humanity where further research into the specific role and mechanism of glucosepane can help scientists gain a deeper understanding of diabetes and aging, so as to find better treatment options.

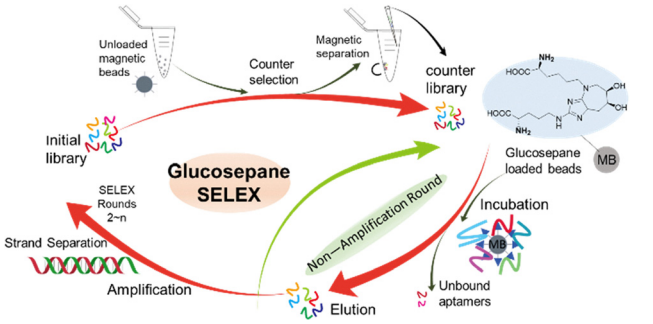


Scheme 1 Schematic overview of the FluMag-SELEX based evolution of a focused glucosepane aptamer library. Initial counter selection by incubation of an initial aptamer library (~$10^{12-16}$ individual aptamers), containing 40 randomized nucleotides flanked by two primer binding sites (23 nt each), with two successive rounds of unloaded tosyl-activated magnetic beads (MB) resulting in an aptamer "counter library" with reduced aptamer amounts with specificity against the carrier material. Selection of focused polyclonal aptamer libraries by SELEX against glucosepane by the reduction of sequence diversity by incubating the counter selected aptamer library first with unloaded beads and subsequently with the glucosepane loaded beads. Aptamers with an adequate three-dimensional structure bind to the target whereas the remaining unbound aptamers are subsequently removed; the bound aptamers are then eluted from glucosepane by heat denaturation and amplified by the PCR and the unwanted complementary strands are removed prior to the following SELEX round. The enriched pool from the previous selection step can either go through the (inner) non-amplification round and be used immediately in the next selection or go through the regular (outer) amplification cycle.

In this work, we present the selection of individual aptamers isolated from an enriched polyclonal (*i.e.* focused) library, which are able to bind glucosepane with high affinity and specificity (Scheme 1). After six rounds of enrichment and selection, the polyclonal library was shown to be functional for glucosepane binding by fluorescent labeling of glucosepane on magnetic particles and allowed purification of glucosepane from solutions. Next-generation sequencing of the final library in combination with bioinformatic analyses delivered 10 individual aptamers, which were chemically synthesized and characterized by the fluorescent labeling assay on magnetic particles and $K_D$ values of the resulting best and worst binding aptamers were determined to be in the low nanomolar range. Both aptamers were then used to demonstrate that aptamers can be used to stain and differentiate tissues in dermal sections of diabetic mice and wild-type (healthy) mice. The robustness and easiness of the presented SELEX-based isolation of specific individual aptamers raised against glucosepane as a major small molecule essential in tissue ageing promises a rise of the aptamer-technology also in immune-histology. Moreover, measuring and determining glucosepane quickly, easily and specifically is crucial because it serves as a key biomarker of aging and age-related diseases. Glucosepane is a major AGE that accumulates in tissues over time, contributing to tissue stiffness, inflammation, and impaired organ function. By accurately assessing glucosepane levels, researchers and clinicians can gain insights into the aging process, monitor the effectiveness of anti-aging or therapeutic interventions, and develop

 This journal is © The Royal Society of Chemistry 2025

Open Access Article. Published on 14 August 2025. Downloaded on 1/24/2026 11:41:00 PM.
This article is licensed under a Creative Commons Attribution 3.0 Unported Licence.

personalized strategies for managing age-related conditions such as cardiovascular diseases, diabetes and neurodegenerative disorders.

## Results and discussion

### Immobilization of glucosepane in tosyl-activated magnetic beads

Glucosepane formation is triggered by a nucleophilic attack of the amino group of the lysine residue by the active carbonyl group of glucose, a reaction commonly referred to as the Maillard reaction. The reaction products are rearranged to form a more stable Amadori product. What follows is a series of reactions where the carbonyl group is transported along the main chain of glucose molecules before cyclization occurs. A further reaction with an amino group on the side chain of an arginine residue forms glucosepane crosslinking.[41,42] Immobilization of glucosepane was performed by covalent coupling of tosyl-activated beads with primary amino groups (Fig. 1(A)). Glucosepane coated magnetic beads were confirmed by eluting the bound molecules and measured by ultraviolet-visible (UV-VIS) spectroscopy. The absorbance of different known concentrations of glucosepane was measured and a standard curve was drawn at the first place (Fig. 1(B)). Following the Lambert–Beer law, a linear fit of the calibration data was used to calculate the amounts of eluted glucosepane from loaded beads (Fig. 1(C)). A calibration curve of the correlation between the glucosepane concentration and the absorbance

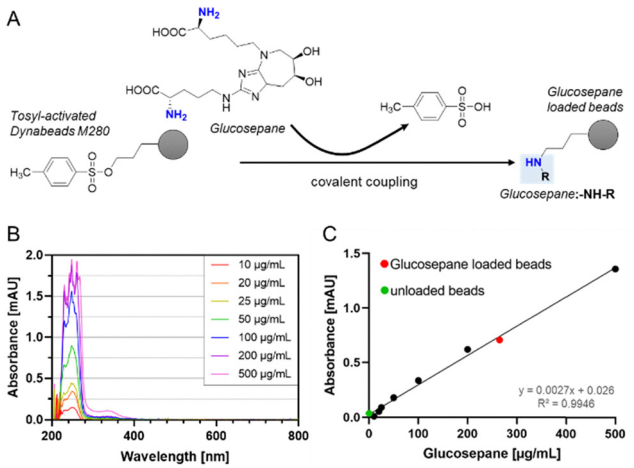


Fig. 1 Covalent coupling of glucosepane to tosyl-activated beads. (A) Schematic illustration of the attachment of glucosepane to tosyl-activated magnetic beads (MB) *via* the amino groups of glucosepane forming covalent amide bonds with tosyl-groups on the surface of the magnetic beads. (B) Through the absorbance measurement of known concentrations (10 µg mL$^{-1}$, 20 µg mL$^{-1}$, 25 µg mL$^{-1}$, 50 µg mL$^{-1}$, 100 µg mL$^{-1}$, 200 µg mL$^{-1}$, and 500 µg mL$^{-1}$) of glucosepane from 200 to 800 nm using an UV-Vis spectrophotometer (Nanodrop 2000c, Thermo Fisher Scientific, Waltham, Massachusetts, USA), the absorbance curves of measured samples at different concentrations are plotted. (C) Linear relationship of the absorbance and sample concentration is presented by linear regression with GraphPad Prism.

was linearly plotted. The sample elution from the loaded bead was regarded as the unknown sample, and the concentration was calculated using a linear equation, which is represented by red/green dots in Fig. 1(C). The concentration of glucosepane eluted from loaded beads was 265 µg mL$^{-1}$, while glucosepane was not detected in unloaded beads as the negative control.

### *In vitro* selection of aptamer libraries against glucosepane

To develop a methodological tool specific to glucosepane, the polyclonal ssDNA aptamer library was evolved through a total of eight rounds of selection during iterative-SELEX. The SELEX cycle was run with increasing stringency by multiplying washing steps after aptamer binding, increasing BSA and tRNA concentrations for blocking unspecific binding, decreasing the aptamer concentration, according to the scheme described in Table S1. Unlike normal SELEX, which comes along with one round of counter SELEX and one round of SELEX with the target, we adopted a non-amplification round as one more SELEX round with targets before the next round of counter SELEX. More SELEX rounds with the target within one round of selection accelerates the SELEX process, saves a lot of time, and makes the SELEX process more efficient. The non-amplification round not only eliminates the amplification step, but also results in a more specific library through one more SELEX with glucosepane loaded beads.

These polyclonal aptamer libraries that bind to glucosepane were successfully selected from a random ssDNA library containing about $6 \times 10^{12}$ individual aptamers with 40 randomized nucleotides flanked by two primer binding sites (23 nt each). Through an early counter-selection process, the use of empty (or "unloaded") magnetic beads to eliminate non-specific oligonucleotides prior to each selection round increases specificity. In each round of selection, the aptamers were Cy5-labeled as labelled PCR primers, followed by fluorescence analysis. To verify the evolution progress, the quantitative PCR (qPCR) was performed with the eluates of the respective SELEX rounds using the fluorescent dye SYBR Green I. The amount of elution aptamers increased with each round of selection, indicating progress in the recovery process (Fig. S1C). In addition, the melting curves of aptamer libraries from SELEX rounds were analyzed in the qPCR. $T_m$ represents the average melting temperature profile, and the melting temperatures $S_{T_m}$ and $E_{T_m}$ at the beginning and end of SELEX are determined, respectively. During the SELEX process, the library melting temperature rose from 63 °C ($S_{T_m}$) to 81 °C ($E_{T_m}$) (Fig. S1A). The effective improvement of the maximum melting temperature of the library is due to the enrichment of DNA aptamers with high GC content in the library, which usually have better secondary structural stability and can provide more potential hydrogen bonds for the target atoms. To compare the degree of shift of the melt curve during screening, we quantified the relative $\mathrm{d}\mathrm{d}R_n/\mathrm{d}T$ values for each screening round at the peak temperatures of $S_{T_m}$ and $E_{T_m}$ to provide a measure of $T_m$ shift during screening, where the $\mathrm{d}\mathrm{d}R_n/\mathrm{d}T$ values gradually decrease at $S_{T_m}$ and, conversely, increase and eventually stabilize at $E_{T_m}$ (Fig. S1B).

Open Access Article. Published on 14 August 2025. Downloaded on 1/24/2026 11:41:00 PM.
This article is licensed under a Creative Commons Attribution 3.0 Unported Licence.

### Specificity and affinity analysis of glucosepane aptamer libraries

The specific binding characteristics of aptamer libraries were examined using glucosepane coated magnetic beads as well as unloaded beads. Therefore, defined amounts of aptamers (5 pmol) from SELEX round 2, 4, and 6 were incubated with unloaded beads and glucosepane-loaded magnetic beads respectively, after the selection process. The libraries Cy5-labeled against unloaded beads and glucosepane-loaded beads were incubated for 30 min at 25 °C and analyzed fluorescently after elution (see Fig. S2A). As expected, the non-specific binding of aptamer libraries decreased and specific binding of aptamer libraries rose with increasing selection rounds (Fig. S2B), but results from polishing counter SELEX round 2 and round 4 showed the abnormally elevated nonspecific binding. The aptamer library R6 obtained in the final productive round showed the highest level of specificity, as expected (Fig. S2C).

In addition, the highly selective target binding of the round 6 aptamer library was further proven by fluorescence microscopy. Here, 5 pmol of the aptamer library was incubated with glucosepane magnetic beads for 30 min, and the unloaded magnetic beads were used as the negative control. Fluorescence could only be detected in the sample containing the glucosepane magnetic beads, confirming the selectivity of the binding process (Fig. S2D).

In order to evaluate the binding strength of the final anti-glucosepane aptamer library R6, the dissociation constant ($K_d$) was determined by co-incubation of increasing amounts of R6 Cy5-labeled aptamers with fixed amounts of glucosepane (Fig. S2E) and found to be very considerable in the lower nanomolar range (30.35 ± 0.51 nM).

### Identification of anti-glucosepane individual aptamers

Our aptamer library R6, evolved after six rounds from FluMag-SELEX, targets glucosepane, allowing specific labelling and differentiation of glucosepane. The technical basis for the analysis and subsequent isolation of individual aptamers in the last round of SELEX is the comparison of round 6 (final) and R3 (early) NGS using Illumina sequencing. An ideal (commercial) synthetic aptamer initiation library should contain an evenly distributed ratio of four nucleobases in the oligonucleotide sequence: adenosine, thymine, cytosine, and guanine. After selection of sequences with enhanced affinity to the desired target, the distribution of individual nucleotides in the entire sequence space changes after analysis, often accompanied by an increase in the GC content.[43] Analysis of the nucleotide distribution of the glucosepane-R3 library revealed typical distributions for an early round of SELEX, each still close to the ideal 25% (Fig. S3A, left). In contrast, in the aptamer library R6, the nucleotide composition showed significant changes, as expected during SELEX evolution and selection to produce higher affinity aptamers (Fig. S3A, right).

Plotting the frequency of individual sequences in the total sequence space of early and final SELEX rounds of NGS reactions (reads per million (RPM)) yields a plot where individual sequences with the same abundance in both rounds are located diagonally. This allows the identification of sequences with the highest total abundance in the last round (glucosepanes 1–6), as well as sequences with the highest enrichment between the early and last round (glucosepanes 7–10). These sequences were selected for chemical synthesis to further characterize these binding molecules (Table S3).

### Characterization of selected individual aptamers

For specificity analyses, the selected individual aptamers were comparatively analyzed with unloaded beads serving as the control, and glucosepane-loaded magnetic beads for specific binding. Compared with the aptamer library R6, the specific binding ability of cyanine-5 labelled fluorescent individual aptamers to glucosepane was higher, which was especially the case for aptamer Glu3 (Fig. 2(A) and (B)). This aptamer also showed the most specific binding towards the target. Aptamer affinity assays were performed again by co-incubating different

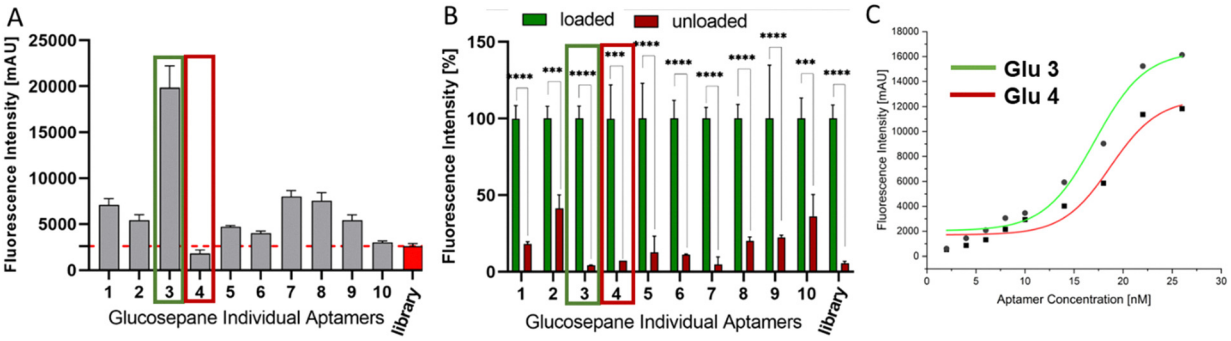


Fig. 2 Fluorescence-based affinity and specificity analyses. (A) Binding assays of individual aptamers Glu1–Glu10 and the aptamer library R6 with glucosepane loaded beads. The red dotted line represents the specific binding strength of the aptamer library R6 and glucosepane. (B) Specificity detection of individual aptamers and the aptamer library R6. The fluorescently labelled aptamers are incubated with glucosepane loaded and unloaded magnetic beads (negative control) separately. Fluorescence intensity can be correlated with the affinity of the aptamers against the given target. Error bars represent the standard deviations of experiments conducted as triplicate ($N$ = 3) and $p$ values $<0.05$ were considered significant. ***$p < 0.001$ and ****$p < 0.0001$. (C) Determination of the dissociation constant for the glucosepane aptamer Glu3 with a $K_d$ value of 17.10 ± 0.96 nM and $R^2$ = 0.9773. Determination of the dissociation constant for the glucosepane aptamer Glu4 with a $K_d$ value of 18.71 ± 1.29 nM and $R^2$ = 0.9633.

Open Access Article. Published on 14 August 2025. Downloaded on 1/24/2026 11:41:00 PM.
This article is licensed under a Creative Commons Attribution 3.0 Unported Licence.

concentrations of aptamer Glu3 (''best'' aptamer) and Glu4 (as the ''worst'' aptamer'') with equal amounts of glucosepane. The aptamer concentration was fitted to the corresponding bound fluorescence intensity by using GraphPad PRISM 8 (GraphPad Software, San Diego, CA, USA) to determine the $K_d$ values of the fluorescent aptamer (Fig. 2(C)). The $K_d$ value was determined to be 17.10 ± 0.96 nM, which indicated that the individual aptamer Glu3 had a higher affinity for glucosepane than the final focused aptamer library R6. Glu4 was the only individual aptamer with lower specificity than the library R6 among the 10 individual aptamers. However, the affinity of Glu4 was demonstrated well with a $K_d$ value of 18.71 ± 1.29 nM.

The Glu3 aptamer showed excellent specificity and affinity for glucosepane, which was further demonstrated in a displacement experiment. To confirm that aptamer binding is not solely dependent on bead-immobilized glucosepane, we performed competition assays in which free glucosepane in solution displaced fluorescently labeled Glu3 pre-bound to glucosepane-coupled beads, as the chemical immobilization may alter the epitope presentation or restrict the conformational flexibility of glucosepane. After the Glu3 aptamer binds to the glucosepane-coated bead, free glucosepane was added to compete with the bound Glu3 aptamer. As the concentration of the added glucosepane increased, the amount of the eluted aptamer increased and accordingly, the amount of the free Glu3 aptamer remaining on the beads gradually decreases. However, free lysine and arginine do not have high enough affinities in order to compete favourably with glucosepane for binding to Glu3 (Fig. 3).

For the sake of determining the maximal binding capacities of the glucosepane aptamers, different defined quantities of amine-labelled aptamer libraries were immobilized on the magnetic beads, incubated with an excess of free glucosepane, and the bound molecules were eluted and measured by UV-VIS spectroscopy (Fig. 4(A) for the schematic overview). First, the absorbance of different known concentrations of glucosepane was measured and a standard curve was plotted (Fig. 4(B)). Measurement of bound glucosepane by incubation with beads loaded with defined amounts of either the anti-glucosepane aptamer library or with the individual aptamer Glu3 revealed that the accurate concentration of eluted glucosepane increases with the aptamer concentration until saturation was reached (Fig. 4(C)). The individual aptamer Glu3 can efficiently bind more glucosepane in total showing greater binding capacity than the final library R6.

In diabetes, prolonged high blood sugar accelerates the formation of glucosepane, which can exacerbate complications such as cardiovascular diseases, kidney dysfunction, and nerve damage. Elevated levels of glucosepane in diabetic patients serve as a biomarker of disease progression and tissue damage, highlighting its role in the pathophysiology of diabetes and its long-term effects on organ functions. Hence, to ultimately show the robustness of Glu3 as a highly specific labelling agent for glucosepane skin biopsies of either healthy wild-type mice and diabetic db/db mice were analyzed. Fluorescence staining was performed on 5-μm thick sections of mouse skin biopsies (from male db/db mice with diabetes and wild-type control mice)

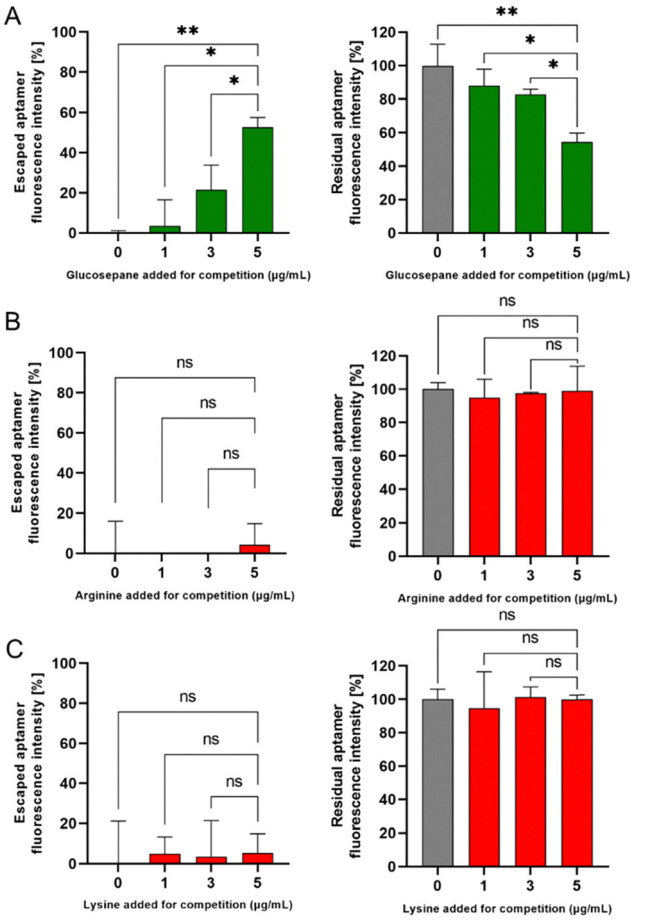


Fig. 3 Anti-glucosepane aptamer displacement by glucosepane as a competitor. The cyanine 5-labelled Glu3 aptamer was bound to glucosepane-loaded magnetic beads and incubated for 30 min at 25 °C. The supernatants were removed, and then the beads were washed with PBS buffer. Different concentrations of (A) glucosepane, (B) arginine and (C) lysine (0 μg mL$^{-1}$, 1 μg mL$^{-1}$, 3 μg mL$^{-1}$, and 5 μg mL$^{-1}$) were incubated with the loaded and aptamer pre-labeled beads. The supernatants were separated by magnetic separation for detection, and the beads were washed with PBS buffer and resuspended in PBS. After elution (95 °C, 5 min), the aptamer solutions were analyzed by monitoring the fluorescence intensity using a Tecan infinite F200 microplate reader (Tecan Group AG, Männedorf, Suisse), and the emission was monitored at 670 nm with an excitation wavelength of 635 nm. Experiments were conducted in triplicates with $p$ values of $<0.05$ were considered significant. *$p < 0.05$ and ** $p < 0.01$, and ns depicts not significant.

adapted from standard immunofluorescence staining protocols, where the paraffin sections were deparaffinized and rehydrated, stained directly using 48 pmol Cy-5 labelled Glu3 or Glu4 aptamers for 1 h at 25 °C, rinsed subsequently to remove unbound aptamers and nuclei were counterstained with DAPI. It could be revealed that under diabetic conditions the best-performer Glu3 can significantly fluorescently distinguish tissues in deeper skin sections, whereas Glu4 does not show any labelling under diabetic conditions and the negative control ATCG[44] did not show any labelling at all (Fig. 5) also under collagen co-stained conditions (Fig. S4).

To our knowledge, we have not only performed the first FluMag-SELEX against glucosepane as one of the most

Open Access Article. Published on 14 August 2025. Downloaded on 1/24/2026 11:41:00 PM.
This article is licensed under a Creative Commons Attribution 3.0 Unported Licence.

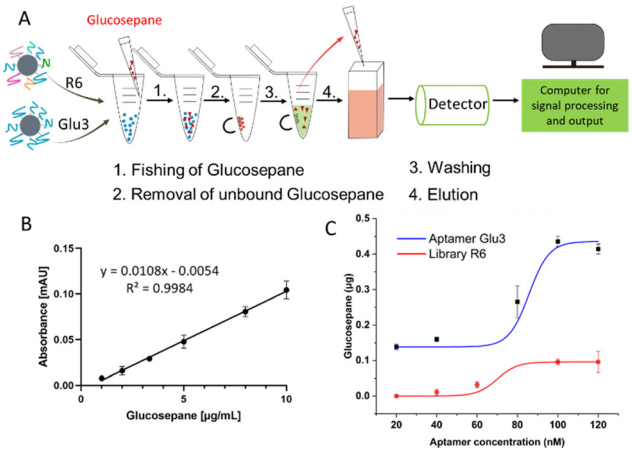


Fig. 4 Magnetic particles functionalized with anti-glucosepane aptamers can extract glucosepane from solution. (A) Schematic overview of the "fishing" assay with anti-glucosepane aptamer loaded magnetic beads. The amino-labelled aptamer library R6 and the individual aptamer Glu3 are loaded on magnetic beads separately, followed by incubation with glucosepane, magnetic separation and resuspension in 1× PBS buffer for washing. The bound glucosepane is then eluted by heat (95 °C for 5 min) and quantified by UV-VIS spectroscopy. (B) Linear relationship of absorbance and the pure glucosepane concentration is presented by linear regression with GraphPad Prism and used as the calibration curve. Error bars indicate standard deviations from experiments conducted as triplicate ($N$ = 3). (C) Glucosepane binding capacities of the final aptamer library R6 and the selected aptamer Glu3 determined by adding fixed amounts of glucosepane and increasing amounts of the aptamer, respectively.

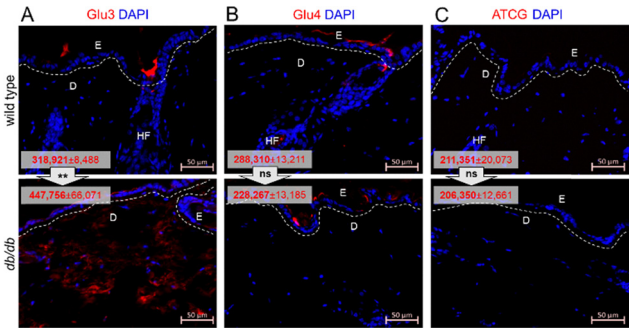


Fig. 5 Comparative representative microphotographs with (A) Glu3, (B) Glu4 and (C) ATCG aptamer mediated fluorescence staining (red) of glucosepane in 5-µm thick sections of mouse skin biopsies from db/db mice with diabetes and wild-type mice with DAPI co-staining (blue). Dashed line indicates the epidermal–dermal junction. Fluorescence images were captured at 20× magnification with a Zeiss Imager.M2 microscope. The scale bar is 50 µm. Red numbers in white boxes indicate mean overall anti-glucosepane aptamer fluorescence intensities determined using ZEN 3.2, Zeiss software from seven ($N$ = 7) equal micrograph areas. Significant differences were marked with asterisk (*) with $p$ values <0.5 being considered as statistically significant, $^{**}p < 0.01$, and ns indicates not significant. Abbreviations: D, dermis; DAPI, 4′,6-diamidino-2-phenylindole; E, epidermis; HF, hair follicle.

prominent AGEs, but have also isolated the first DNA aptamer specifically binding glucosepane on magnetic particles and in solution with a dissociation constant of 17.1 nM (aptamer Glu3). This aptamer could be used in a histological staining procedure similar to immunohistological methods traditionally being based on primary antibodies in combination with labelled secondary antibodies. Although such antibody-dependent protocols usually require prolonged experimental processing times involving long incubation and blocking steps, which typically can account for a total of approximately 20 hours,[21,45,46] the aptamer-dependent protocol presented here allowed to circumvent blocking and the whole procedure could be completed within 2.5 hours. In addition, the staining was direct using the fluorescently labelled aptamer without the need of a secondary antibody. Despite the promising performance of Glu3 *in vitro* and in murine tissue sections, further evaluation of aptamer specificity within complex tissue environments is necessary, as the presence of other AGEs (*e.g.* Nε-carboxymethyllysine, Nε-carboxyethyllysine or pentosidine)[47,48] and extracellular matrix components may potentially affect aptamer binding. While our competition assays confirmed selectivity for glucosepane over structurally similar molecules such as lysine and arginine, future studies will include additional *in situ* controls, such as aptamer pre-incubation with excess free glucosepane or staining of tissue sections pre-treated to reduce matrix complexity and to rigorously assess potential cross-reactivity with other (structurally similar) AGEs and/or extracellular matrix components. Moreover, although this study provides a strong proof-of-concept in the diabetic mouse skin and wild-type mouse skin, validation in human clinical tissue remains a critical step towards clinical translation.[49] Murine and the human skin differ substantially in several histological and physiological aspects, including the epidermal thickness, dermal collagen architecture and ECM composition.[50,51] Moreover, the dynamics and localization of AGE accumulation can vary across species due to differences in lifespan, metabolic rate and glycemic history.[52,53] For example, glucosepane crosslinking in human dermal collagen occurs over decades, leading to cumulative and spatially heterogeneous accumulation that may not be fully captured in mouse models with relatively short lifespans and more uniform tissue remodeling.[39,40,54] We also demonstrated that the Glu3 aptamer effectively binds glucosepane in paraffin-embedded skin sections, indicating that the aptamer remains functional despite common processing steps such as formalin fixation and paraffin embedding.[55] However, it is well known that such procedures can alter the structural integrity of target epitopes or mask binding sites, particularly for non-antibody probes such as aptamers, which rely on defined three-dimensional folding for target recognition. Factors such as fixation duration, embedding temperature and antigen retrieval protocols may influence the accessibility of glucosepane or the folding stability of the aptamer.[56] Despite these current limitations, our findings establish a strong basis for the further development of glucosepane-targeting aptamers as histological tools. Future studies will expand validation across species, tissue types and processing protocols (*e.g.* frozen *vs.* paraffin-embedded sections), ultimately aiming for robust applications in clinical diagnostics and therapeutic monitoring. With this study, we

 This journal is © The Royal Society of Chemistry 2025

Open Access Article. Published on 14 August 2025. Downloaded on 1/24/2026 11:41:00 PM.
This article is licensed under a Creative Commons Attribution 3.0 Unported Licence.

not only have introduced the first anti-glucosepane aptamer, but have also added another example to the portfolio of histological staining procedures. The ease of selection of an appropriate aptamer against an intended target as well as the ease of the aptamer-based histological staining procedure in combination with the possibility to omit secondary binding molecules not only make this application probably faster, but also can promise economical affordability. This may also provide researchers and clinicians with a novel tool to gain insight into the role of glucosepane in the aging process, to monitor the effectiveness of anti-aging or therapeutic interventions and help to develop personalized strategies for managing age-related conditions such as cardiovascular diseases, diabetes and neurodegenerative disorders in the future.

## Conflicts of interest

There are no conflicts to declare.

## Data availability

Data generated by NG Sequencing for the analyses and selection of the individual aptamers used in the study are deposited online under the following file name "Li *et al.*_SELEX Sequencing Glucosepane.gz" and are accessible using this link: **https://cloudstore.uni-ulm.de/s/4P8aiNGzSmWgPSX**.

Supplementary information available: Detailed materials and methods information, SELEX and aptamer sequencing results and tissue stainings are available. See DOI: **https://doi.org/10.1039/d5nh00263j**

## Acknowledgements

This work was supported by the China Scholarship Council (No. 202408080088) and also by the Gesellschaft für Forschungsförderung (GFF) of Lower Austria as part of the project "Aptamers and Odorant Binding Proteins – Innovative Receptors for Electronic Small Ligand Sensing" (FTI22-G-012). This work was also supported by the Austrian Research Promotion Agency (FFG) within the COMET Project "PI-SENS" (project no. 915477) as well as by the Federal Provinces of Lower Austria and Tirol. K. S. K. was supported by the Deutsche Forschungsgemeinschaft (DFG, German Research Foundation) – CRC1506, Project-ID 450627322 "Aging at Interfaces" and SFB 1149, Project-ID 251293561 "Trauma"– Project-C5.

## References

1 A. D. Ellington and J. W. Szostak, *Nature*, 1990, **346**, 818–822.
2 C. Tuerk and L. Gold, *Science*, 1990, **249**, 505–510.
3 R. Stoltenburg, N. Nikolaus and B. Strehlitz, *J. Anal. Methods Chem.*, 2012, 415697.
4 C. Lyu, I. M. Khan and Z. Wang, *Talanta*, 2021, **229**, 122274.
5 X. Liu, Y. Hou, Y. Qin, J. Cheng, J. Hou, Q. Wu and Z. Liu, *Biosensors*, 2023, **13**, 564.
6 W. Guo, C. Zhang, T. Ma, X. Liu, Z. Chen, S. Li and Y. Deng, *J. Nanobiotechnol.*, 2021, **19**, 1–19.
7 W. Zhong, Y. Pu, W. Tan, J. Liu, J. Liao, B. Liu, K. Chen, B. Yu, Y. Hu, Y. Deng, J. Zhang and H. Liu, *Anal. Chem.*, 2019, **91**, 8289–8297.
8 L. Li, J. Wan, X. Wen, Q. Guo, H. Jiang, J. Wang, Y. Ren and K. Wang, *Anal. Chem.*, 2021, **93**, 7369–7377.
9 A. Kusumawati, A. Z. Mustopa, I. W. T. Wibawan, A. Setiyono and M. B. Sudarwanto, *J. Genet. Eng. Biotechnol.*, 2022, **20**(1), 95.
10 K. Sefah, D. Shangguan, X. Xiong, M. B. O'Donoghue and W. Tan, *Nat. Protoc.*, 2010, **5**, 1169–1185.
11 K. Murakami, N. Izuo and G. Bitan, *J. Biol. Chem.*, 2022, **298**(1), 101478.
12 J. Yang and M. T. Bowser, *Anal. Chem.*, 2013, **85**, 1525–1530.
13 R. Stoltenburg, C. Reinemann and B. Strehlitz, *Anal. Bioanal. Chem.*, 2005, **383**, 83–91.
14 A. K. Kissmann, J. Andersson, A. Bozdogan, V. Amann, M. Krämer, H. Xing, H. F. Raber, D. H. Kubiczek, P. Aspermair, W. Knoll and F. Rosenau, *Nanoscale Horiz.*, 2022, **7**, 770–778.
15 V. Lucarelli, D. Colbert, S. Li, M. Cumming, W. Linklater, J. Mitchell, J. Travas-Sejdic and A. Kralicek, *Talanta*, 2022, **240**, 123073.
16 C. Lu, C. Liu, Q. Zhou, X. Chen, H. Li, S. Wang and Y. Guo, *Anal. Chim. Acta*, 2022, **1191**, 339291.
17 A. S. Sadeghi, M. Mohsenzadeh, K. Abnous, S. M. Taghdisi and M. Ramezani, *Talanta*, 2018, **182**, 193–201.
18 Y. Zhang, H. Xing, R. Li, J. Andersson, A. Bozdogan, R. Strassl, B. Draphoen, M. Lindén, M. Henkel, U. Knippschild, R. Hasler, C. Kleber, W. Knoll, A. K. Kissmann and F. Rosenau, *Adv. Healthcare Mater.*, 2024, **14**(4), 2403827.
19 H. Xing, Y. Zhang, R. Li, H. M. Ruzicka, C. Hain, J. Andersson, A. Bozdogan, M. Henkel, U. Knippschild, R. Hasler, C. Kleber, W. Knoll, A. K. Kissmann and F. Rosenau, *Nanoscale Horiz.*, 2025, **10**, 124–134.
20 B. M. Bachtiar, C. Srisawat, R. P. Rahayu, R. D. Soedjodono, S. A. Prabandari and E. W. Bachtiar, *Eur. J. Dent.*, 2022, **16**, 543–548.
21 J. A. Gabriel, N. Weerasinghe, P. Balachandran, R. Salih and G. E. Orchard, *Br. J. Biomed. Sci.*, 2024, **81**, DOI: **10.3389/BJBS.2024.13437**.
22 S. Van Noorden, *Folia Histochem. Cytobiol.*, 2002, **40**, 121–124.
23 V. M. Monnier, *Arch. Biochem. Biophys.*, 2003, **419**, 1–15.
24 D. R. Sell, K. M. Biemel, O. Reihl, M. O. Lederer, C. M. Strauch and V. M. Monnier, *J. Biol. Chem.*, 2005, **280**, 12310–12315.
25 J. Bjorksten and H. Tenhu, *Exp. Gerontol.*, 1990, **25**, 91–95.
26 M. Segel, B. Neumann, M. F. E. Hill, I. P. Weber, C. Viscomi, C. Zhao, A. Young, C. C. Agley, A. J. Thompson, G. A. Gonzalez, A. Sharma, S. Holmqvist, D. H. Rowitch, K. Franze, R. J. M. Franklin and K. J. Chalut, *Nature*, 2019, **573**, 130–134.
27 W. Wang, E. M. Lollis, F. Bordeleau and C. A. Reinhart-King, *FASEB J.*, 2019, **33**, 1199–1208.

Open Access Article. Published on 14 August 2025. Downloaded on 1/24/2026 11:41:00 PM.
This article is licensed under a Creative Commons Attribution 3.0 Unported Licence.

28 P. MJ, Z. Q, F. A, H. C, L. TR, M. PH, M. MF and L. FS, *J. Am. Soc. Nephrol.*, 2006, **17**, 2640–2643.
29 C. Legrand, U. Ahmed, A. Anwar, K. Rajpoot, S. Pasha, C. Lambert, R. K. Davidson, I. M. Clark, P. J. Thornalley, Y. Henrotin and N. Rabbani, *Arthritis Res. Ther.*, 2018, **20**, 131.
30 V. M. Monnier, S. Genuth and D. R. Sell, *Glycoconjugate J.*, 2016, **33**, 569–579.
31 J. S. Sjöberg and S. Bulterijs, *Rejuvenation Res.*, 2009, **12**, 137–148.
32 M. J. Fazio, D. R. Olsen and J. J. Uitto, *Cutis*, 1989, **43**, 437–444.
33 J. Qvist, S. E. Johansson and L. M. Johansson, *Scand. J. Soc. Med.*, 1996, **24**, 67–76.
34 H. Takbkoshi, S. I. Kitamura, K. Matsuoka, Y. Atsmui, A. Horiuchi, S. Akatsuka, T. Ishii, Y. Hosoda and Y. Watanabe, *Tohoku J. Exp. Med.*, 1983, **141**, 523–528.
35 H. Sumino, S. Ichikawa, M. Abe, Y. Endo, O. Ishikawa and M. Kurabayashi, *J. Am. Geriatr. Soc.*, 2004, **52**, 945–949.
36 S. J. Lai-Fook and R. E. Hyatt, *J. Appl. Physiol.*, 2000, **89**, 163–168.
37 P. De Vita and T. Hortobagyi, *J. Gerontol., Ser. A*, 2000, **55**, B593–B600.
38 N. A. Calcutt, M. E. Cooper, T. S. Kern and A. M. Schmidt, *Nat. Rev. Drug Discovery*, 2009, **8**, 417–430.
39 V. M. Monnier, W. Sun, D. R. Sell, X. Fan, I. Nemet and S. Genuth, *Clin. Chem. Lab. Med.*, 2014, **52**, 21–32.
40 V. M. Monnier, D. R. Sell, C. Strauch, W. Sun, J. M. Lachin, P. A. Cleary and S. Genuth, *J. Diabetes Complications*, 2013, **27**, 141–149.
41 K. M. Bieme, D. Alexander Fried and M. O. Lederer, *J. Biol. Chem.*, 2002, **277**, 24907–24915.
42 K. M. Biemel, O. Reihl, J. Conrad and M. O. Lederer, *J. Biol. Chem.*, 2001, **276**, 23405–23412.
43 A. K. Kissmann, G. Bolotnikov, R. Li, F. Müller, H. Xing, M. Krämer, K. E. Gottschalk, J. Andersson, T. Weil and F. Rosenau, *Appl. Microbiol. Biotechnol.*, 2024, **108**(1), 284.
44 A.-K. Kissmann, G. Bolotnikov, R. Li, F. Müller, H. Xing, M. Krämer, K.-E. Gottschalk, J. Andersson, T. Weil and F. Rosenau, *Appl. Microbiol. Biotechnol.*, 2024, **108**, 284.
45 P. Maity, K. Singh, L. Krug, A. Koroma, A. Hainzl, W. Bloch, S. Kochanek, M. Wlaschek, M. Schorpp-Kistner, P. Angel, A. Ignatius, H. Geiger and K. Scharffetter-Kochanek, *Cell Rep.*, 2021, **36**(9), 109634.
46 K. Singh, P. Maity, A. K. Koroma, A. Basu, R. K. Pandey, S. Vander Beken, P. Haas, L. Krug, A. Hainzl, A. Sindrilaru, C. Pfeiffer, M. Wlaschek, N. Y. Frank, M. H. Frank, C. Ganss, A. Bánvölgyi, N. Wikonkál, S. Eming, I. Pastar, M. Tomic-Canic, M. A. Kluth and K. Scharffetter-Kochanek, *J. Invest. Dermatol.*, 2022, **142**, 1725–1736.
47 N. M. J. Hanssen, L. Engelen, I. Ferreira, J. L. J. M. Scheijen, M. S. Huijberts, M. M. J. van Greevenbroek, C. J. H. van der Kallen, J. M. Dekker, G. Nijpels, C. D. A. Stehouwer and C. G. Schalkwijk, *J. Clin. Endocrinol. Metab.*, 2013, **98**, E1369–E1373.
48 J. H. Meertens, H. L. Nienhuis, J. D. Lefrandt, C. G. Schalkwijk, K. Nyyssönen, J. J. M. Ligtenberg, A. J. Smit, J. G. Zijlstra and D. J. Mulder, *PLoS One*, 2016, **11**, e0160893.
49 S. Liu, Y. Xu, X. Jiang, H. Tan and B. Ying, *Biosens. Bioelectron.*, 2022, **208**, 114168.
50 P. A. Gerber, B. A. Buhren, H. Schrumpf, B. Homey, A. Zlotnik and P. Hevezi, *Biol. Chem.*, 2014, **395**, 577–591.
51 H. D. Zomer and A. G. Trentin, *J. Dermatol. Sci.*, 2018, **90**, 3–12.
52 A. Tyshkovskiy, S. Ma, A. V. Shindyapina, S. Tikhonov, S.-G. Lee, P. Bozaykut, J. P. Castro, A. Seluanov, N. J. Schork, V. Gorbunova, S. E. Dmitriev, R. A. Miller and V. N. Gladyshev, *Cell*, 2023, **186**, 2929–2949.
53 P. Baker, C. M. Cooper-Mullin and A. G. Jimenez, *Comp. Biochem. Physiol., Part A:Mol. Integr. Physiol.*, 2022, **267**, 111164.
54 A. Nash, M. Notou, A. F. Lopez-Clavijo, L. Bozec, N. H. de Leeuw and H. L. Birch, *Matrix Biol. Plus*, 2019, **4**, 100013.
55 J. A. Ramos-Vara, J. D. Webster, D. DuSold and M. A. Miller, *Vet. Pathol.*, 2014, **51**, 102–109.
56 V. Denti, I. Piga, S. Guarnerio, F. Clerici, M. Ivanova, C. Chinello, G. Paglia, F. Magni and A. Smith, *J. Am. Soc. Mass Spectrom.*, 2020, **31**, 1619–1624.

 This journal is © The Royal Society of Chemistry 2025